

Room temperature nonvolatile optical control of polar order in a charge density wave

QM Liu,^{1*} Dong Wu,^{2*†} TY Wu,¹ SS Han,² YR Peng,³ ZH Yuan,⁴ YH Cheng,¹
 BH Li,² TC Hu,¹ Li Yue,¹ SX Xu,¹ RX Ding,¹ Ming Lu,² RS Li,¹ SJ Zhang,¹
 BQ Lv,⁵ Alfred Zong,⁶ YF Su,⁷ Nuh Gedik,⁷ ZP Yin,³ Tao Dong,¹ NL Wang^{1,2†}

¹International Center for Quantum Materials, School of Physics, Peking University,
 Beijing 100871, China

²Beijing Academy of Quantum Information Sciences, Beijing 100913, China

³Department of Physics and Center for Advanced Quantum Studies, Beijing Normal University,
 Beijing 100875, China

⁴School of Physics and Information Engineering, Shanxi Normal University, Taiyuan 030031—China

⁵Tsung-Dao Lee Institute, Shanghai Jiao Tong University, Shanghai 200240, China

⁶Department of Chemistry, University of California, Berkeley, California 94720, USA

⁷Department of physics, Massachusetts Institute of Technology, Cambridge, Massachusetts 02139, USA

*These authors contributed equally to this paper

†To whom correspondence should be addressed; E-mail: wudong@baqis.ac.cn;nlwang@pku.edu.cn

Utilizing ultrafast light-matter interaction to manipulate electronic states of quantum materials is an emerging area of research in condensed matter physics. It has significant implications for the development of ultrafast electronic devices of the future. However, the ability to induce long-lasting metastable electronic states yet in a fully reversible manner is a long standing challenge. Here, by using ultrafast laser excitation with distinct pulse sequences and fluences, we were able to regulate the symmetry and electronic properties in a polar

charge-density-wave material EuTe_4 . We demonstrated the capability of non-volatile writing and erasing the polar order, a process that is completely reversible and is achieved at room temperature in an all optical manner. Each induced state brings about modifications to the electric resistance and second harmonic generation intensity. The results point to a distinct dynamical symmetry inversion mechanism in which photoexcitation mediates the polar phases of long-range electronic order. Our finding extends the scope of non-volatile all-optical control of electronic states to ambient conditions, thus providing possibilities for applications in ultrafast optoelectronics.

Introduction

Materials that exhibit long-range electronic order lie at the heart of condensed matter physics and usually display emergent states such as multiferroics, charge density waves (CDW), and high-temperature superconductivity. Photo-induced metastable states are a common occurrence in these systems, but they are usually short-lived and revert to their initial states within a few picoseconds to microseconds through a combination of electronic, thermal, and lattice relaxation processes [1, 5, 6, 7, 9, 11, 14, 23, 28]. When the photoinduced states persist permanently, i.e., in a nonvolatile way, the phenomena have attracted particular interests and are considered technologically significant. Recent advances have revealed a few cases of ultrafast photoinduced nonvolatile electronic order transitions at low temperatures in quantum materials, where the underlying lattice remains intact [26, 27, 33], which have deeply expanded our understanding of nonequilibrium dynamics. However, despite their advances, the nonvolatile optical control of electronic states at ambient conditions is still a long sought-after issue, in particular in an all-optical reversible manner.

In another aspect, ultrafast photon excitation has been observed to cause a switch in lattice

inversion symmetry, which can potentially alter the macroscopic state and physical properties of a material. Examples of this include the inversion symmetry switching in SrTiO₃, which induced a hidden ferroelectric phase [16, 19]; in an organic charge-transfer crystal, leading to a transition from the ground neutral state to an ionic ferroelectric state [4]; and in Weyl semimetals WTe₂ and MoTe₂, where it caused a transition from the noncentrosymmetric topological Weyl state to the centrosymmetric trivial state [23, 34]. The cooperative interaction between electronic and structural relaxation processes of the optically excited states creates a new symmetry with long-range electronic order switching. This optical approach to manipulating symmetry is intriguing for ultrafast generation of exotic quantum states and may find rich applications in memory devices [22], novel topological functionality [24, 30], and unconventional superconductivity [18, 20].

Here we report the discovery of nonvolatile all-optical manipulation of the electronic states at room temperature in EuTe₄ - a rare polar CDW semiconductor characterized by a lack of inversion symmetry. We focused on femtosecond above-gap excitation and monitored the inversion symmetry through second harmonic generation (SHG) experiments. The results showed a remarkable ultrafast photoinduced nonvolatile symmetry switching, allowing reversible generation and removal of the polar order through optical means alone. Our findings, combined with Ginzburg-Landau simulations, suggest distinct roles of photo-control in the phase inversion within the polar CDW order of EuTe₄.

EuTe₄ is a quasi-two-dimensional semiconducting CDW material [17, 29]. Its crystal structure consists of layers of planar Te sheets separated by insulating EuTe slabs (Fig. 1a). Below $T_c \sim 652$ K and at room temperature, the CDW distortion of square Te- sheets yields an incommensurate CDW with a near $1 a \times 3 b \times 2 c$ superlattice [17, 21]. In the Te sheets, the incommensurate CDW is formed with the CDW modulation q pointing along the b -axis, which is perpendicular to its polarization vector e (the direction of the Te atomic displacement, along

the a -axis; Fig. 1b). These combined atomic displacements lead to the Te-bond rearrangement and the formation of the regular in-plane Te-trimers. As a result of this CDW distortion, the in-plane inversion symmetry of the Te-sheet is broken in the a -axis direction (the right panel of Fig. 1b). In other words, the Te-trimers formation collectively contributes a net polarization along the a -axis direction in a single CDW Te-sheet. Such an improper polarization [3] of the Te-sheet is a slave property of the CDW order. As shown in the schematic of Fig 1.c, parallel alignment of the polarization of the Te-sheets between adjacent layers leads to spatial inversion symmetry breaking along the a -axis and hence a polar order in the EuTe_4 CDW state.

In the experiments reported here, EuTe_4 was excited with 800 nm femtosecond optical pulses from a Ti: Sapphire laser amplifier system with a pulse duration of 35 fs at the repetition rate of 1 kHz (Materials and Methods). A writing beam was set up and served to induce phase transitions (Fig. 1d). Structural symmetry information was monitored by continuously rotating the linear polarization of the incoming 800-nm pulse and measuring the emitted 400-nm second harmonic projected into the a - b plane along the [001] crystallographic direction with a second polarizer. The electrical resistance was monitored by the four-electrode method. We select a near-normal-incidence optical geometry, thus SHG light probes the in-plane symmetry property (supplementary text S1). The measured angle-dependent SHG spectra indicate the formation of polarization along the [1 0 0] direction already at room temperature, consistent with the XRD measured noncentrosymmetric polar point group ($2mm$) for CDW EuTe_4 (Fig. S1). Detailed SHG measurements show typical thermal hysteresis behavior upon cooling and heating processes (Fig. 1e), where the hysteresis follows the same trend as the ones found in the curves of temperature-dependent resistivity and CDW superlattice peak intensity [17, 29].

Nonvolatile all-optical electronic state switching at room temperature

The optical experiments were performed as a function of incident fluence in nanometer-thick EuTe_4 samples (Materials and Methods). To take an overview of the photoinduced effects, as seen in Figs. 2 and 3, a laser writing pulse was possible to suppress or enhance the SHG signal with the electric resistivity switched concomitantly, dependent on the starting state and pump fluence. The phenomena were found to be prominent already at room temperatures and remained detectable up to 350 K (Fig. S2). The photoinduced phase was nonvolatile and remained indefinitely (verified up to 3 weeks) when the writing pulse is turned off.

We found there exist two typical excitation regimes separated by a threshold $F_{cR} \sim 6.8 \text{ mJ/cm}^2$ of the writing pulse intensity (marked as Regime-W for weak excitations and Regime-S for strong excitations, see Fig.2 and Fig.3 respectively, see more details for F_{cR} in Fig. S3 and supplementary text S2). Below F_{cR} (Regime-W) and for the initial state at cooling branch 300 K case, the application of a single writing pulse will result in the establishment of a nonvolatile state characterized by an increase in both resistance magnitude and SHG intensity (Fig. 2a, b). The maximum values of these quantities are attained at an incident intensity approximately 1.5 mJ/cm^2 (Fig. 2e, f red curves). Beyond this intensity, the application of single writing pulse induces states characterized by a gradual decrease in both resistance and SHG values, culminating in complete suppression of SHG intensity above fluence of approximately 4 mJ/cm^2 (Fig. 2e red curves). Yet for the starting state at temperature 300 K of the heating branch, the application of a single writing pulse will tend to suppress the resistance magnitude and the SHG intensity (Fig. 2c,d). Interestingly, both the spectra starting from different thermal branches display a rather gradual threshold in writing fluence (Fig. 2e,f). This implies that for intermediate excitation densities, only a variable part of the volume is switched to the nonvolatile state. Em-

pirically, for the Regime-W, we found that the complete removal of the photoinduced state can be effectively achieved by means of thermal annealing, resulting in the system reverting back to its original ground state (See more details in Fig. S4 and supplementary text S3).

Once the writing fluence rises above the F_{cR} , a new nonvolatile hidden phase (Regime-S) was created. As seen in Fig. 3, for the excitation energy exceeds F_{cR} , a state with orders-of-magnitude larger resistivity was reached, and the SHG intensity was below the experimental detection limit. Subsequently, using the same writing beam but with reduced energy (in a range of $4 - 5 \text{ mJ/cm}^2$), a train of thousands of writing pulses will drive a new polar state showing low resistivity and distinct SHG pattern (Fig. 3b,c). The analysis of this new SHG pattern indicates a strongly enhanced nonlinear susceptibility tensor χ_{aaa} (See more details in supplementary text S1, S4, Fig. S5, S6, Table.S1). We ascribe this photoinduced hidden state to a dynamics that photoexcitations above F_{cR} exert a strong light-matter interaction and induce a further distortion to Te-trimers along a -axis irreversibly, then the subsequent moderate excitations drive those trimers polarized; the stronger distortion of the Te-trimers of polar state, the stronger χ_{aaa} susceptibility tensor. In Regime-S, a new way of all-optical rewritable phase transition can be found: a single-shot pulse with energy above F_{cR} will drive the system into a nonpolar state characterized with zero SHG and gigantic resistivity, then the subsequent pulses with reduced energy will drive the system to revert to a polar state characterized with intense SHG signal and low resistivity (Fig. 3b,c). We note here that a large energy barrier must exist between various nonvolatile states, which might be stored in the domain walls or in the states themselves, providing the strong stabilization force and keep the induced states nonvolatile against thermal excitations even above room temperatures. This energy barrier can be seen in both the phases of Regimes-W and Regimes-S by examining the thresholds required for triggering the nonvolatile states switching (Fig. 2e, Fig. S7).

To gain insights into the microscopic dynamics of the exotic nonvolatile states in the EuTe_4

system, we investigated both the pristine and photoinduced states with time-resolved SHG and pump-probe spectroscopy. Fig. 4a displays ultrafast measurements of the second harmonic signal as a function of the pump-probe delay for different pump intensities at the original heating branch. After the incidence of the pump pulse, the SHG signal displayed a sharp drop followed by three-step relaxation processes: a positive increase process at the subpicosecond time scale, then a negative relaxation process likely originating from electron-lattice energy transfer within the ~ 3 ps time scale, and finally a slow lattice relaxation that degraded more and more slowly as the pump intensity crossed ~ 1.8 mJ/cm² until diverging at the nonvolatile phase transition (See more details in supplementary text S5, Fig. S8). This typical relaxation process suggests that the nonvolatile phase transition occurs through the electron-lattice interaction process at a time constant of ~ 2.2 ps (see supplementary Fig. S7). No oscillatory signatures of the optical phonon reflecting the possible atomic polar displacement are observed from SHG spectra, in contrast to studies on most other polar/ferroelectric materials where Raman-active phonons can be found from SHG spectra [16, 19, 23].

Time-resolved reflectivity $\Delta R/R(t)$ spectroscopy was performed to characterize the single-particle and collective excitations for various nonvolatile phases following the writing pulses, with the pump and probe pulse energies kept low (< 50 $\mu\text{J}/\text{cm}^2$ and < 10 $\mu\text{J}/\text{cm}^2$ respectively) to guarantee minimal state disruption. Fig.4b shows $\Delta R/R(t)$ spectroscopy together with their Fourier transforms for various writing intensities, where the coherent phonons are Raman active. We noticed that though the writing intensities lie in a wide range that various nonvolatile states were induced, neither phonon frequency shifting nor phonon number changes could be recognized from the spectra. Furthermore, by checking with transmission electron microscopy (TEM) experiments, the in-plane CDW modulation was found maintained in an unified period for all nonvolatile phases (supplementary text S6, Fig. S9). The above facts indicate that the electronic excitations drive the SHG drastically but without substantial changes in $\Delta R/R(t)$ and

the related frequency spectra, implying that the underlying mechanism of the photoinduced phase transition in EuTe_4 is hidden from the detectable responses of Raman-active excitations (See following discussions).

Thus, some notable features of the photoinduced nonvolatile states in EuTe_4 can be concluded: (1) Photoexcitations above certain thresholds can induce a polar phase and inversion symmetry transformation; (2) After photoexcitation, the system enters nonvolatile states after electron-lattice are in quasi-equilibrium; (3) There are no coherent modulations observed in time-resolved SHG spectra, neither substantial phonon frequency shifting nor phonon number change are detectable from reflectivity spectra; (4) The in-plane CDW modulation remains for the nonvolatile states.

The scenario of nonvolatile phase switching in EuTe_4 and the Ginzburg - Landau simulations

From geometrical principles, the emergence of final polarization in EuTe_4 is mainly contingent on the relative stacking sequence [13, 15, 25, 31] between the adjacent Te-sheets. As is illustrated in the bottom panel of Fig. 5a, for the polarization direction along a -axis, various stacking sequence of adjacent Te-sheets can in principle lead to either a global non-centrosymmetric polar CDW state ($\Psi = 1$) or a centrosymmetric nonpolar CDW state ($\Psi = -1$), where $\Psi = \cos(\phi)$ is the order parameter of the polarization, and $\phi = 0, \pi$ is for in-phase and out-phase stacking respectively (supplementary text S7, Fig. S10, S11). Our crystallographic modeling based on the measured XRD data suggests that these two phases are bistable in structure (supplementary Table S2).

We then propose a scenario of photoinduced polar phase transition, and give a phenomenological simulation based on the theory of a spatially dependent Ginzburg - Landau potential [2, 8, 12, 32] (supplementary text S8). We take the phases of excitation regime-S for example.

The symmetry switch between the noncentrosymmetric polar phase and the centrosymmetric nonpolar phase in the regime-S is understood within the simulated potential energy model of the transition, which is described in terms of a bistable energy surface with two energy minima, as the protocol summarized in Fig. 5a (see more details in Fig. S12). By the Ginzburg - Landau simulation, we confirmed that at certain writing fluences, the macroscopic polar $\Psi = 1$ or non-polar $\Psi = -1$ domains perpendicular to the sample surface can be inverted within a thickness thinner than the optical penetration depth (~ 19 nm, Fig.5b, supplementary text S8). Accordingly, various volume ratios of the two type polarization domains will result in different SHG intensities. As the simulation result shown in Fig. 5c, starting from the nonpolar phase with zero SHG, a fluence exceeding a certain threshold F_{cL} will induce gradually the polar phase with the SHG approaching a constant magnitude. Further increase of the fluence across the threshold F_{cH} will, however, suppress the SHG signals. This spatially dependent simulation of photoinduced phase inversion well captures the trend of fluence dependence and the threshold characteristics detected by SHG measurements. Similar scenario and simulation results of photoinduced phase transformation can also be applied to the phases of Regime-W given relative low energy barriers.

Additionally, in view of the improper polarization characteristics of CDW sheet in EuTe_4 , the direction of the CDW polarization intrinsically belongs to a typical phase of the CDW order parameter of the phase mode (supplementary text S8). Thus, our observations of polar state transition correspond basically to the relative CDW phase mode change, the process does not necessarily require melting the CDW order. Essentially, the phase-mode excitation directly affects the translational motion of the CDW condensate but does not cause the excitation of optical phonons [10]. Therefore, the photoinduced drastic polar phase transition in EuTe_4 is not likely to be Raman sensitive, which is well in agreement with the results of our spectral experiments shown in Fig. 4.

Considering the merits of nonvolatility, ambient conditions, all-optical manipulation, electronic order, and reversible symmetry switching, our finding in EuTe_4 has potential for device applications. The finding is a rare example and will further motivate the search for new generations of room-temperature nonvolatile memory elements in electronically ordered materials. Moreover, our results suggest that the phase part of the order parameter can play a core role in ultrafast control of electronically ordered states, which may be applicable to a wide range of quantum materials far beyond our specific case of EuTe_4 , such as emergent 2D ferroics, topological insulators, strongly-correlated materials, and high- T_c superconductors.

Materials and Methods

Sample growth and device fabrication EuTe_4 single crystals were grown via a solid-phase reaction with Te as the flux. A more detailed description of the reaction process can be found in reference [29]. The quasi two-dimensional (2D) crystals are approximately $5 \times 3 \times 0.2$ mm in size and have mirrorlike surfaces with multiple distinct stripes along a-axis. EuTe_4 flakes (20~50 nm in thickness) used in the experiments were mechanically exfoliated from bulk crystals and then transferred onto sapphire (0 0 1) substrates. The samples were in (0 0 1) plane with a surface area of about $300 \times 300 \mu\text{m}$ and oriented with a-axis along the horizontal direction. The four electrodes ($\sim 30 \mu\text{m}$ apart) for electrical measurements were fabricated through standard ultra-violet lithography and electron beam evaporation with 10 nm Ti and 80 nm Au being deposited on the sample successively.

Experimental Method All the ultrafast laser beams were derived from the Ti: Sapphire Amplifier system (Spitfire Ace) of which the center wavelength, pulse duration and repetition rate were 800 nm, 35 fs and 1 kHz respectively. A single laser pulse, used as writing/erasing beam, was extracted from the original pulse train by using a timing delay generator that was synchronized with laser source and an electronic shutter. The samples were mounted on a

liquid-He flow optical cryostat (Oxford Instruments) equipped with silica window.

For the resistance measurements, the writing beam was focused on the sample from back side with a spot diameter of about $700\ \mu\text{m}$ to make sure that the sample was completely covered. Photoinduced stable changes of resistance were recorded in situ using Keithley 2400 Source-Meter through standard four-electrode technique. The constant current through the sample was set to $1\ \mu\text{A}$ and the voltage between two middle electrodes was monitored. Temperature dependence of resistance in the original and photoinduced nonvolatile states was measured on physical property measurement system (PPMS, Quantum Design).

For static/time-resolved second harmonic generation (SHG) measurements in reflection geometry, the propagation direction of both the pump and probe beams were oriented normal to ab plane (0 0 1) of the sample (along c-axis) with probe beam departure from c-axis at a small angle (roughly 7 degree). The spot diameters of the pump and probe beam at sample position were $800\ \mu\text{m}$ and $350\ \mu\text{m}$, respectively. The probe fluence was set to $0.15\ \text{mJ}/\text{cm}^2$. The incident probe light (800 nm) was tuned to circularly polarized light using a quarter waveplate and then its polarization control was achieved by rotating a linear polarizer. Another rotatable linear polarizer on the outgoing beam was used for analysis of different measurement channels. The reflected second harmonic (400 nm) signal was collected using a photomultiplier tube photodetector (PMT, PMM01, Thorlabs, Bias voltage set as 0.65 V) after passing by short-pass and bandpass filter groups. The output of the PMT was sent to a lock-in amplifier with modulation of 373 Hz by a mechanical chopper. A tunable attenuator in the pump beam was used for fluence dependence measurements. The polarization of pump light was tuned by a half wave plate.

For the time-resolved reflectivity spectra measurements, the same reflection geometry as the above SHG experiments was used. The fluence of the probe beam was smaller than $0.1\ \text{mJ}/\text{cm}^2$. The polarization of pump (along b-axis) and probe (along a-axis) kept perpendicular

to each other. Besides, the balanced detection was achieved using two Si free-space amplified photodetectors.

References

- [1] C. Bao, P. Tang, D. Sun, and S. Zhou. Light-induced emergent phenomena in 2D materials and topological materials. *Nature Reviews Physics*, 4(1):33–48, 2022. ISSN 25225820. doi: 10.1038/s42254-021-00388-1.
- [2] P. Beaud, A. Caviezel, S. O. Mariager, L. Rettig, G. Ingold, C. Dornes, S. W. Huang, J. A. Johnson, M. Radovic, T. Huber, T. Kubacka, A. Ferrer, H. T. Lemke, M. Chollet, D. Zhu, J. M. Glowonia, M. Sikorski, A. Robert, H. Wadati, M. Nakamura, M. Kawasaki, Y. Tokura, S. L. Johnson, and U. Staub. A time-dependent order parameter for ultrafast photoinduced phase transitions. *Nature Materials*, 13(10):923–927, 2014. ISSN 14764660. doi: 10.1038/nmat4046.
- [3] E. Bousquet, M. Dawber, N. Stucki, C. Lichtensteiger, P. Hermet, S. Gariglio, J. M. Triscone, and P. Ghosez. Improper ferroelectricity in perovskite oxide artificial superlattices. *Nature*, 452(1):732–736, 2008. ISSN 1476-4687. doi: 10.1038/nature06817.
- [4] E. Collet, M.-H. Lemée-Cailleau, M. B.-L. Cointe, H. Cailleau, M. Wulff, T. Luty, S.-Y. Koshihara, M. Meyer, L. Toupet, P. Rabiller, and S. Techert. Laser-induced ferroelectric structural order in an organic charge-transfer crystal. *Science*, 300(5619):612–615, 2003. doi: 10.1126/science.1082001. URL <https://www.science.org/doi/abs/10.1126/science.1082001>.
- [5] A. De La Torre, D. M. Kennes, M. Claassen, S. Gerber, J. W. McIver, and M. A. Sentef. Colloquium: Nonthermal pathways to ultrafast control in quantum materials. *Reviews of*

- Modern Physics*, 93(4):41002, 2021. ISSN 15390756. doi: 10.1103/RevModPhys.93.041002. URL <https://doi.org/10.1103/RevModPhys.93.041002>.
- [6] A. S. Disa, J. Curtis, M. Fechner, A. Liu, A. von Hoegen, M. Först, T. F. Nova, P. Narang, A. Maljuk, A. V. Boris, B. Keimer, and A. Cavalleri. Photo-induced high-temperature ferromagnetism in YTiO₃. *Nature*, 617(1):73–78, 2023. ISSN 1476-4687. doi: 10.1038/s41586-023-05853-8.
- [7] T. Dong, S. J. Zhang, and N. L. Wang. Recent Development of Ultrafast Optical Characterizations for Quantum Materials. *Advanced Materials*, pages 1–46, 2022. ISSN 15214095. doi: 10.1002/adma.202110068.
- [8] S. Duan, Y. Cheng, W. Xia, Y. Yang, C. Xu, F. Qi, C. Huang, T. Tang, Y. Guo, W. Luo, D. Qian, D. Xiang, J. Zhang, and W. Zhang. Optical manipulation of electronic dimensionality in a quantum material. *Nature*, 595(7866):239–244, 2021. ISSN 14764687. doi: 10.1038/s41586-021-03643-8. URL <http://dx.doi.org/10.1038/s41586-021-03643-8>.
- [9] D. Fausti, T. RI, N. Dean, S. Kaiser, A. Dienst, H. MC, S. Pyon, T. T, H. Takagi, and A. Cavalleri. Light-Induced Superconductivity in a Stripe-Ordered Cuprate. *Science*, 331(1):189–191, 2011. ISSN 0036-8075. doi: 10.1126/science.1197294.
- [10] G. Grüner. The dynamics of charge-density waves. *Rev. Mod. Phys.*, 60:1129–1181, Oct 1988. doi: 10.1103/RevModPhys.60.1129. URL <https://link.aps.org/doi/10.1103/RevModPhys.60.1129>.
- [11] J. G. Horstmann, H. Böckmann, B. Wit, F. Kurtz, G. Storeck, and C. Ropers. Coherent control of a surface structural phase transition. *Nature*, 583(1):232–236, 2020. ISSN 14764687. doi: 10.1038/s41586-020-2440-4.

- [12] T. Huber, S. O. Mariager, A. Ferrer, H. Schäfer, J. A. Johnson, S. Grübel, A. Lübcke, L. Huber, T. Kubacka, C. Dornes, C. Laulhe, S. Ravy, G. Ingold, P. Beaud, J. Demsar, and S. L. Johnson. Coherent structural dynamics of a prototypical charge-density-wave-to-metal transition. *Phys. Rev. Lett.*, 113:026401, Jul 2014. doi: 10.1103/PhysRevLett.113.026401. URL <https://link.aps.org/doi/10.1103/PhysRevLett.113.026401>.
- [13] J. Ji, G. Yu, C. Xu, and H. J. Xiang. General theory for bilayer stacking ferroelectricity. *Phys. Rev. Lett.*, 130:146801, Apr 2023. doi: 10.1103/PhysRevLett.130.146801. URL <https://link.aps.org/doi/10.1103/PhysRevLett.130.146801>.
- [14] A. Kogar, A. Zong, P. E. Dolgirev, X. Shen, J. Straquadine, Y. Q. Bie, X. Wang, T. Rohwer, I. C. Tung, Y. Yang, R. Li, J. Yang, S. Weathersby, S. Park, M. E. Kozina, E. J. Sie, H. Wen, P. Jarillo-Herrero, I. R. Fisher, X. Wang, and N. Gedik. Light-induced charge density wave in LaTe₃. *Nature Physics*, 16(2):159–163, 2020. ISSN 17452481. doi: 10.1038/s41567-019-0705-3.
- [15] L. Li and M. Wu. Binary Compound Bilayer and Multilayer with Vertical Polarizations: Two-Dimensional Ferroelectrics, Multiferroics, and Nanogenerators. *ACS Nano*, 11(6): 6382–6388, 2017. ISSN 1936086X. doi: 10.1021/acsnano.7b02756.
- [16] X. Li, T. Qiu, J. Zhang, E. Baldini, J. Lu, A. M. Rappe, and K. A. Nelson. Terahertz field-induced ferroelectricity in quantum paraelectric SrTiO₃. *Science*, 364(6445): 1079–1082, 2019. ISSN 10959203. doi: 10.1126/science.aaw4913.
- [17] B. Q. Lv, A. Zong, D. Wu, A. V. Rozhkov, B. V. Fine, S.-D. Chen, M. Hashimoto, D.-H. Lu, M. Li, Y.-B. Huang, J. P. C. Ruff, D. A. Walko, Z. H. Chen, I. Hwang, Y. Su, X. Shen, X. Wang, F. Han, H. C. Po, Y. Wang, P. Jarillo-Herrero, X. Wang,

- H. Zhou, C.-J. Sun, H. Wen, Z.-X. Shen, N. L. Wang, and N. Gedik. Unconventional hysteretic transition in a charge density wave. *Phys. Rev. Lett.*, 128:036401, Jan 2022. doi: 10.1103/PhysRevLett.128.036401. URL <https://link.aps.org/doi/10.1103/PhysRevLett.128.036401>.
- [18] M. R. Norman. The challenge of unconventional superconductivity. *Science*, 332(6026):196–200, 2011. doi: 10.1126/science.1200181. URL <https://www.science.org/doi/abs/10.1126/science.1200181>.
- [19] T. F. Nova, A. S. Disa, M. Fechner, and A. Cavalleri. Metastable ferroelectricity in optically strained SrTiO₃. *Science*, 364(6445):1075–1079, 2019. ISSN 10959203. doi: 10.1126/science.aaw4911.
- [20] X.-L. Qi and S.-C. Zhang. Topological insulators and superconductors. *Rev. Mod. Phys.*, 83:1057–1110, Oct 2011. doi: 10.1103/RevModPhys.83.1057. URL <https://link.aps.org/doi/10.1103/RevModPhys.83.1057>.
- [21] R. Rathore, A. Pathak, M. K. Gupta, R. Mittal, R. Kulkarni, A. Thamizhavel, H. Singhal, A. H. Said, and D. Bansal. Evolution of static charge density wave order, amplitude mode dynamics, and suppression of kohn anomalies at the hysteretic transition in eut_{e4}. *Phys. Rev. B*, 107:024101, Jan 2023. doi: 10.1103/PhysRevB.107.024101. URL <https://link.aps.org/doi/10.1103/PhysRevB.107.024101>.
- [22] J. F. Scott and C. A. P. de Araujo. Ferroelectric memories. *Science*, 246(4936):1400–1405, 1989. doi: 10.1126/science.246.4936.1400. URL <https://www.science.org/doi/abs/10.1126/science.246.4936.1400>.
- [23] E. J. Sie, C. M. Nyby, C. D. Pemmaraju, S. J. Park, X. Shen, J. Yang, M. C. Hoffmann, B. K. Ofori-Okai, R. Li, A. H. Reid, S. Weathersby, E. Mannebach, N. Finney, D. Rhodes,

- D. Chenet, A. Antony, L. Balicas, J. Hone, T. P. Devereaux, T. F. Heinz, X. Wang, and A. M. Lindenberg. An ultrafast symmetry switch in a Weyl semimetal. *Nature*, 565(1): 61–66, 2019. ISSN 1476-4687. doi: 10.1038/s41586-018-0809-4.
- [24] N. Sirica, P. P. Orth, M. S. Scheurer, Y. M. Dai, M. C. Lee, P. Padmanabhan, L. T. Mix, S. W. Teitelbaum, M. Trigo, L. X. Zhao, G. F. Chen, B. Xu, R. Yang, B. Shen, C. Hu, C. C. Lee, H. Lin, T. A. Cochran, S. A. Trugman, J. X. Zhu, M. Z. Hasan, N. Ni, X. G. Qiu, A. J. Taylor, D. A. Yarotski, and R. P. Prasankumar. Photocurrent-driven transient symmetry breaking in the Weyl semimetal TaAs. *Nature Materials*, 21(1):62–66, 2022. ISSN 14764660. doi: 10.1038/s41563-021-01126-9.
- [25] M. V. Stern, Y. Waschitz, W. Cao, I. Nevo, K. Watanabe, T. Taniguchi, E. Sela, M. Urbakh, O. Hod, and M. B. Shalom. Interfacial ferroelectricity by van der Waals sliding. *Science*, 372(6549):1462–1466, 2021. doi: doi:10.1126/science.abe8177. URL <https://www.science.org/doi/abs/10.1126/science.abe817>.
- [26] L. Stojchevska, I. Vaskivskyi, T. Mertelj, P. Kusar, D. Svetin, S. Brazovskii, and D. Mihailovic. Ultrafast switching to a stable hidden quantum state in an electronic crystal. *Science*, 344(6180):177–180, 2014. ISSN 10959203. doi: 10.1126/science.1241591.
- [27] S. W. Teitelbaum, B. K. Ofori-Okai, Y.-H. Cheng, J. Zhang, F. Jin, W. Wu, R. D. Averitt, and K. A. Nelson. Dynamics of a persistent insulator-to-metal transition in strained manganite films. *Phys. Rev. Lett.*, 123:267201, Dec 2019. doi: 10.1103/PhysRevLett.123.267201. URL <https://link.aps.org/doi/10.1103/PhysRevLett.123.267201>.
- [28] Y. H. Wang, H. Steinberg, P. Jarillo-Herrero, and N. Gedik. Observation of floquet-bloch states on the surface of a topological insulator. *Science*, 342(6157):453–457, 2013.

- doi: 10.1126/science.1239834. URL <https://www.science.org/doi/abs/10.1126/science.1239834>.
- [29] D. Wu, Q. M. Liu, S. L. Chen, G. Y. Zhong, J. Su, L. Y. Shi, L. Tong, G. Xu, P. Gao, and N. L. Wang. Layered semiconductor eute_4 with charge density wave order in square tellurium sheets. *Phys. Rev. Mater.*, 3:024002, Feb 2019. doi: 10.1103/PhysRevMaterials.3.024002. URL <https://link.aps.org/doi/10.1103/PhysRevMaterials.3.024002>.
- [30] L. X. Yang, Z. K. Liu, Y. Sun, H. Peng, H. F. Yang, T. Zhang, B. Zhou, Y. Zhang, Y. F. Guo, M. Rahn, D. Prabhakaran, Z. Hussain, S.-K. Mo, C. Felser, B. Yan, and Y. L. Chen. Weyl semimetal phase in the non-centrosymmetric compound TaAs. *Nature Physics*, 11(9):728–732, 2015. ISSN 1745-2481. doi: 10.1038/nphys3425. URL <https://doi.org/10.1038/nphys3425>.
- [31] K. Yasuda, X. Wang, K. Watanabe, T. Taniguchi, and P. Jarillo-Herrero. Stacking-engineered ferroelectricity in bilayer boron nitride. *Science*, 372(6549):1458–1462, 2021. doi: 10.1126/science.abd3230. URL <https://www.science.org/doi/abs/10.1126/science.abd3230>.
- [32] R. Yusupov, T. Mertelj, V. V. Kabanov, S. Brazovskii, P. Kusar, J. H. Chu, I. R. Fisher, and D. Mihailovic. Coherent dynamics of macroscopic electronic order through a symmetry breaking transition. *Nature Physics*, 6(9):681–684, 2010. ISSN 17452481. doi: 10.1038/nphys1738. URL <http://dx.doi.org/10.1038/nphys1738>.
- [33] J. Zhang, X. Tan, M. Liu, S. W. Teitelbaum, K. W. Post, F. Jin, K. A. Nelson, D. N. Basov, W. Wu, and R. D. Averitt. Cooperative photoinduced metastable phase control in

strained manganite films. *Nature Materials*, 15(9):956–960, 2016. ISSN 14764660. doi: 10.1038/nmat4695.

- [34] M. Y. Zhang, Z. X. Wang, Y. N. Li, L. Y. Shi, D. Wu, T. Lin, S. J. Zhang, Y. Q. Liu, Q. M. Liu, J. Wang, T. Dong, and N. L. Wang. Light-induced subpicosecond lattice symmetry switch in mote_2 . *Phys. Rev. X*, 9:021036, May 2019. doi: 10.1103/PhysRevX.9.021036. URL <https://link.aps.org/doi/10.1103/PhysRevX.9.021036>.

Acknowledgments

This work was supported by NSFC (No. 11888101, 12274033, 12374063, 23Z990202580), National Key Research and Development Program of China (No. 2022YFA1403901, 2021YFA1400201), Shanghai Natural Science Fund for Original Exploration Program (23ZR1479900), US Department of Energy (Basic Energy Sciences, Materials Sciences and Engineering Division-data analysis), the Gordon and Betty Moore Foundation’s EPIQS Initiative grant GBMF9459 (instrumentation).

Fig. 1

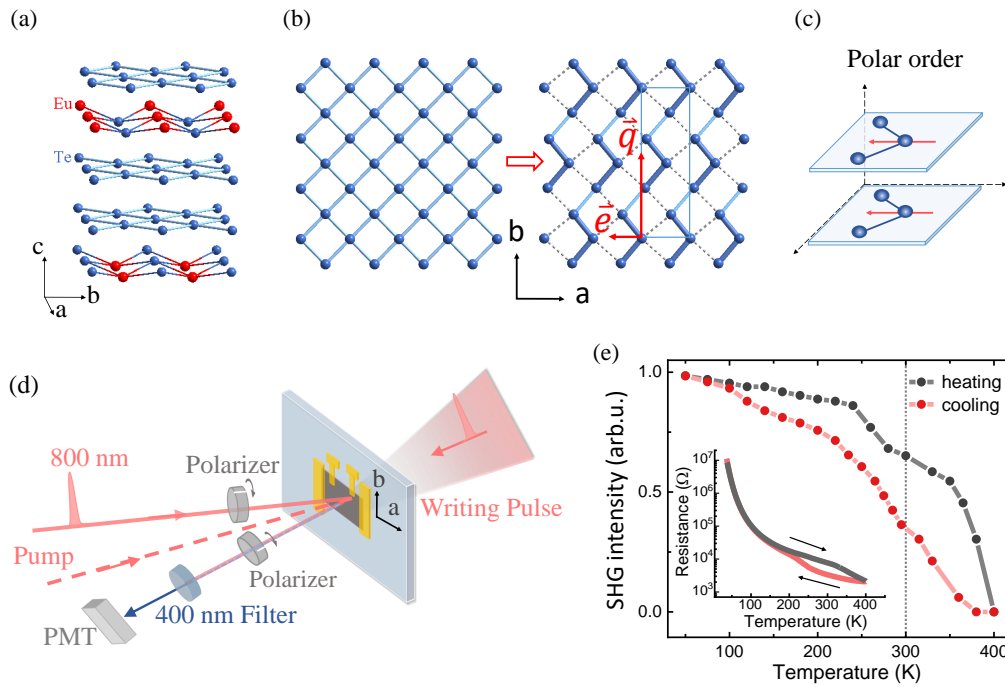


Figure 1: **Schematic description of photo-control of polar electronic state of EuTe₄.** (a) The averaged crystal structure of EuTe₄, which contains the layered Te square lattices. (b) The Peierls instability of square Te-sheet leads to the formation of distorted Te-trimers. The CDW vector q points along the b -axis, which is perpendicular to its polarization vector e . For a single Te-sheet, the in-plane inversion symmetry breaking can be carefully recognized from the right panel. (c) The schematic of stacking sequence of the polarized Te-sheets for the formation of the polar order in EuTe₄, with the Te-trimers from the adjacent Te-sheets pointing to the same direction. (d) Sketch of the experimental setup. Where the PMT denotes photomultiplier tube photodetector. (e) The measured second harmonic intensity as the function of temperature. The spectra show typical thermal hysteresis behavior upon cooling and heating processes, which is coincident closely to the hysteresis behavior found in the spectra of resistance (the inset).

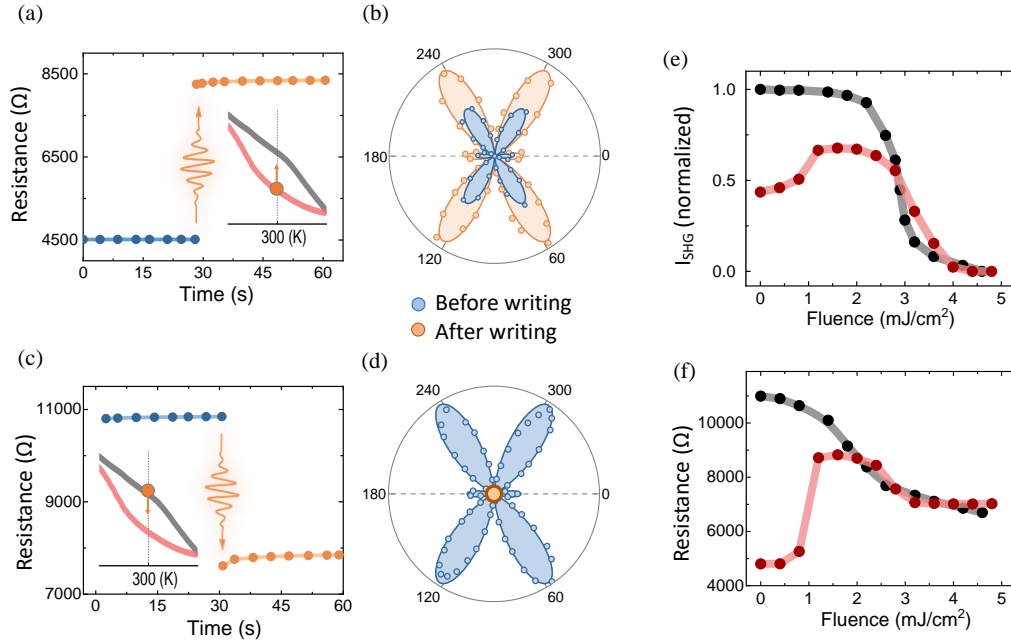


Figure 2: **Nonvolatile SHG and resistivity switching by a 35-fs laser pulse at 800 nm in the weak excitation regime.** Below $F_{cR} \sim 6.8 \text{ mJ/cm}^2$, a single shot writing pulse can enhance or suppress both the resistivity values and SHG magnitude, dependent on the writing intensity and the annealing history branch. **(a, b)** Starting from the state at cooling branch 300 K (see the inset), a single shot weak pulse, e.g., 1.5 mJ/cm^2 , can enhance **(a)** the resistance value and **(b)** the SHG magnitude simultaneously. **(c, d)** At heating branch 300 K, a single shot intense pulse, e.g., 4.5 mJ/cm^2 , can suppress both **(c)** the resistance and **(d)** SHG magnitudes. **(e)** The shot-to-shot SHG intensity and **(f)** the resistance magnitude as a function of writing pulse fluence. The black denotes the excitations starting from the initial state at heating branch 300 K, and the red from cooling branch 300 K.

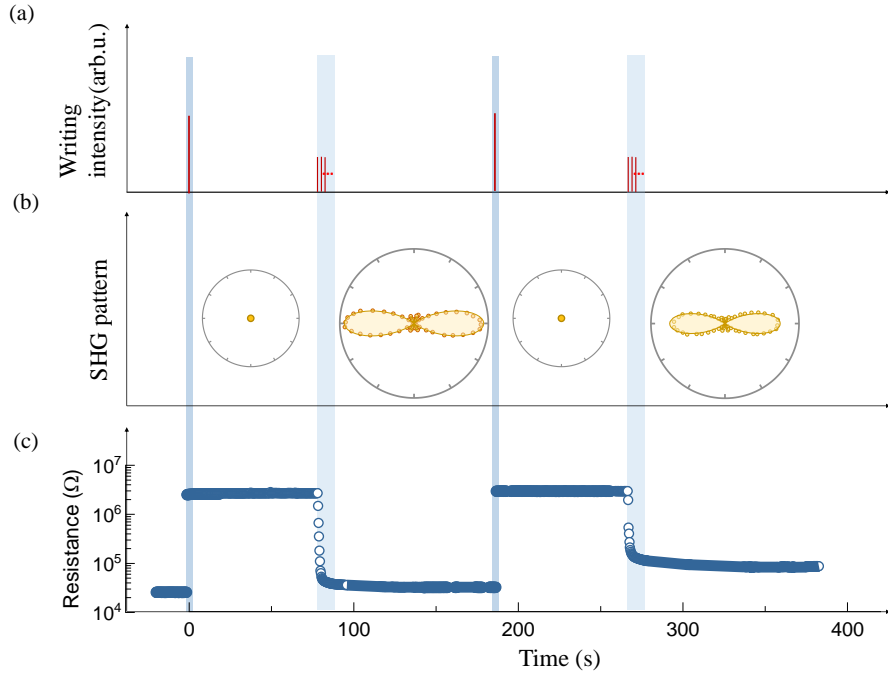


Figure 3: **Nonvolatile SHG and resistivity switching under high excitations in the strong excitation regime.** A high excitation intensity above F_{cR} will drive the system into a new hidden nonvolatile phase regime of Regime-S. **(a)** Depiction of the writing intensities used in sequence, with the strong intensity $\sim 7.5 \text{ mJ/cm}^2$, then the subsequent moderate intensity $\sim 4.5 \text{ mJ/cm}^2$. **(b)** The measured SHG switching after the writing pulses corresponding to **(a)**. Here in the Regime-S, the new SHG pattern will be generated for the moderate excitations. **(c)** The sharp resistance switching correspondingly.

Fig. 4

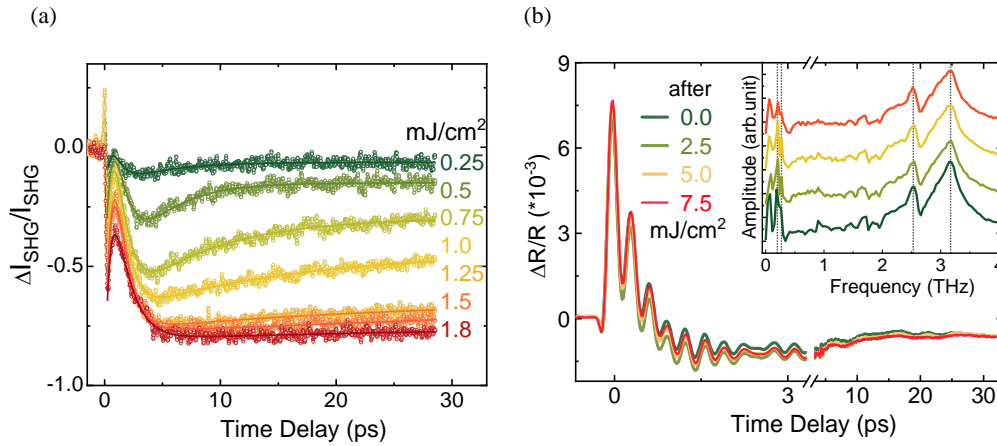


Figure 4: **Time-resolved spectral features of the electronic states in EuTe_4 .** (a) Ultrafast measurements of the second harmonic spectra at various pump fluences for the phase at initial heating branch 300 K before the nonvolatile phase transition induced. (b) Time-resolved reflectivity spectra measured after various writing intensities. The inset are the corresponding Fourier-transformed spectra using the same color notation. The dashed are guidelines.

Fig. 5

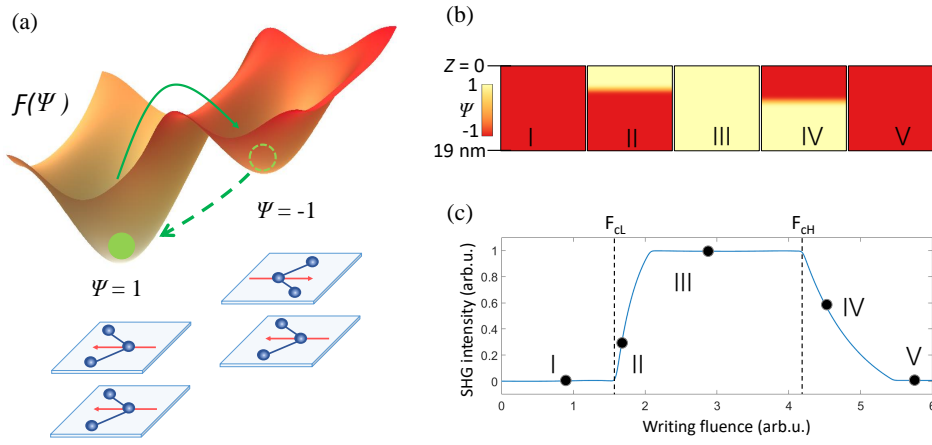


Figure 5: **Simulated photoinduced nonvolatile switching.** (a) (upper panel) Schematic drawing of photoinduced transition between polar ($\Psi = 1$) and non-polar ($\Psi = -1$) phases reversibly in free energy landscape $F(\Psi)$; (bottom panel) different stacking sequence of the CDW Te-sheets can in principle result in either a global non-centrosymmetric polar CDW state ($\Psi = 1$) or a centrosymmetric non-polar CDW state ($\Psi = -1$), where $\Psi = \cos(\phi)$, $\phi = 0, \pi$ is the relative phase of Te-bilayer for in-phase and out-phase stacking respectively. (b) Simulated photoinduced spatial domains distribution perpendicular to the sample surface at certain writing fluences (denoted by the black dots in (c)), where Z depicts the depth from the sample surface. (c) The simulated photoinduced SHG evolution as the function of pulse intensities. The dashed are guidelines.